J Nanopart Res (2016) 18:348
DOI 10.1007/s11051-016-3652-2

RESEARCH PAPER

Two choices for the functionalization of silica nanoparticles with gallic acid: characterization of the nanomaterials and their antimicrobial activity against *Paenibacillus larvae*

Tamara A. Vico · Valeria B. Arce · María F. Fangio · Liesel B. Gende · Celso A. Bertran · Daniel O. Mártire · María S. Churio

Received: 5 July 2016 / Accepted: 30 October 2016

Abstract Silica nanoparticles attached to gallic acid were synthesized from 7-nm diameter fumed silica particles by different functionalization methods involving the condensation of hydroxyl or carboxyl groups. The particles were characterized by thermal analyses and UV–vis, FTIR, NMR, and EPR spectroscopies. In comparison to free gallic acid, enhanced stability and increased antimicrobial activity against *Paenibacillus larvae* were found for the functionalized nanoparticles. Thus, both derivatization strategies result in improved properties of the natural polyphenol as antimicrobial agent for the treatment of honeybee pathologies.

Keywords Silica · 3-aminopropyl-triethoxysilane · Phenolic acid · American foulbrood · *Paenibacillus larvae* · Semiquinone radicals · Nanoparticles · Microbiology

Introduction

Considerable efforts are currently devoted to the development of new materials aimed to decrease the problems generated by the extensive use of antibiotics. In this sense, naturally occurring antimicrobial agents represent an interesting choice with reduced potential

Electronic supplementary material The online version of this article (doi:10.1007/s11051-016-3652-2) contains supplementary material, which is available to authorized users.

T. A. Vico · M. F. Fangio · M. S. Churio
Departamento de Química, FCEyN/IFIMAR, CONICET, Universidad Nacional de Mar del Plata, Funes 3350, B7602AYL Mar del Plata, Argentina

V. B. Arce
Centro de Investigaciones Ópticas (CIOp), CONICET La Plata—CIC—UNLP, Camino Centenario y 506, C.C. 3, Gonnet, 1897, La Plata, Argentina

M. F. Fangio (✉) · M. S. Churio (✉)
Instituto de Investigaciones Físicas de Mar del Plata (IFIMAR), CONICET, Universidad Nacional de Mar del Plata, Funes 3350, 7600, Mar del Plata, Argentina
e-mail: mfangio@mdp.edu.ar
e-mail: schurio@mdp.edu.ar

L. B. Gende
Centro de Investigaciones en Abejas Sociales, FCEyN, Universidad Nacional de Mar del Plata, Funes 3350, 7600, Mar del Plata, Argentina

C. A. Bertran
Chemistry Institute, University of Campinas, Caixa Postal 615, Campinas, SP 13083-970, Brazil

D. O. Mártire
Instituto de Investigaciones Fisicoquímicas Teóricas y Aplicadas (INIFTA), CONICET, Universidad Nacional de La Plata, Diagonal 113 y calle 64, 1900, La Plata, Argentina

Published online: 22 November 2016

impact on the environment and health (Borges et al. 2013). This is an especially relevant condition in the field of beekeeping, where the problems associated with the prolonged use of antibiotics are the reduction of bee's lifetimes, the increased risk of resistant strain emergence, and the contamination of hive products with chemical residues that affect their quality and safety for human consumption (Genersch, 2010; Antúnez et al. 2008). Thus, while oxytetracycline hydrochloride (OTC) is generally used to treat a honeybee larvae disease named American foulbrood (AFB), caused by the endospore-forming bacteria *Paenibacillus larvae*, the antibiotic is banned for the same purpose in most European countries (Genersch, 2010). On the other hand, natural products such as propolis extracts (which contain phenolic acids, flavonoids, terpenes, and essential oils) have been proved to be effective in the control of AFB (Antúnez et al. 2008).

Polyphenolic compounds in general, and particularly gallic acid (3,4,5-trihydroxybenzoic acid, GA), are good antimicrobial agents which also show antioxidant capacity (Borges et al. 2013; Marino et al. 2014). However, one of the main concerns about their use is its sensitivity to environmental factors such as light, heat, and oxygen (Fang and Bhandaria 2010). In fact, GA and analog plant polyphenols are susceptible to autoxidation in aqueous solution in the presence of oxygen (Mochizuki et al. 2002; Friedman and Jurgens 2000).

Various approaches, including the association to different nanostructured matrixes, have been explored with the purpose of increasing the stability and conserving the bioactivity of this substance (Fang and Bhandaria 2010). GA has been bonded to organic polymers such as gelatin and chitosan (Cirillo et al. 2010; Cho et al. 2011), and included in cyclodextrins (Olga et al. 2015) or linked to inorganic materials, for example silica nanoparticles (Deligiannakis et al. 2012; Hu et al. 2013). In particular, silica nanoparticles have the advantage of being a cheap inert material from the biochemical point of view to which the GA can be chemically bonded on the surface to generate a functionalized nanoparticle. A highly efficient antioxidant hybrid nanomaterial results when GA is covalently grafted to aminopropyl-SiO_2 nanoparticles by amide bonds with the carboxyl group of the phenolic acid (Deligiannakis et al. 2012). However, the condensation of the silanol groups with phenolic hydroxyls has not been explored for GA (Ruiz et al. 2007; Escalada et al. 2014). This strategy could offer an interesting alternative for the functionalization of the SiO_2 which may allow the assessment of structure-activity connections since the potential of phenolic acids to inhibit microbial growth has been found to be influenced by the number of hydroxyl groups and substituents on the aromatic ring (Borges et al. 2015; Sanchez-Maldonado et al. 2011).

In the present work, we achieved the modification of silica nanoparticles surface by linking GA through two different binding sites: the carboxyl and the hydroxyl moieties, with the aim of characterizing and comparing both nanomaterials in terms of their stability, radical production ability, and antimicrobial capacity against the bacteria *Paenibacillus larvae.*

Experimental

Chemicals GA monohydrate (purum >98%) was purchased from Panreac (Barcelona, Spain). Fumed silica (Sigma, specific surface area (SSA) = 390 ± 40 $m^2\ g^{-1}$, particle diameter estimated from the SSA = 7 nm) was dried in a crucible at 120 °C for 15 h and then in a muffle at 250 °C for 3 h and stored in a desiccator. The chemicals N,N-dicyclohexylcarbodiimide (DDC); N-hydroxysuccinimide; KH_2PO_4 and K_2HPO_4 (all from Sigma-Aldrich); CaH_2 (Fluka); and the solvents *o*-xylene, toluene, methanol, ethanol, acetone (all from J.T. Baker for use in HPLC), and ethyl acetate (Cicarelli) were used without further purification. For the studies on the antimicrobial activity, Mueller-Hinton broth, yeast extract, and agar were from Britania, and glucose (Merck), sodium pyruvate (Stanton Ind. Argentina) and OTC (Lab. Key Words) were used.

Modified nanoparticles with the 3-aminopropyltriethoxysilane (APTES) group were synthesized as described by Arce et al. (2015).

Synthesis of the nanoparticles SiO_2 nanoparticles covalently functionalized with GA were prepared by two different approaches. One of the methods involved condensation of the silanol groups with the phenolic

hydroxyls of GA to produce GAO-NP (Eq. (1) (Ruiz et al. 2007).

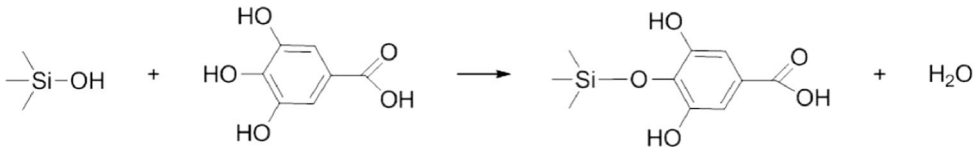

(1)

Alternatively, condensation of the carboxyl group of the phenolic acid with the aminopropyl moiety group of APTES was used to yield silica nanoparticles with covalent attachment to GA through an amide bond (GACON-NP) (Eq. (2) (Deligiannakis et al. 2012). Details of the respective synthetic procedures are given in the following sections.

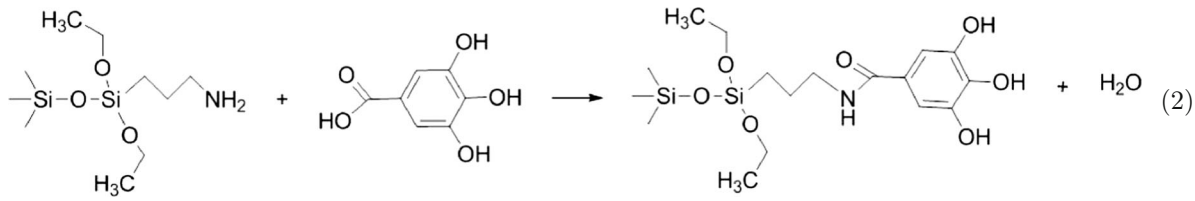

(2)

Synthesis of the GAO-NP The synthesis was performed in a Soxhlet extractor containing CaH_2. Four grams of GA and 180 mL of *o*-xylene were added to 3 g of activated commercial silica nanoparticles and refluxed in 24 h. The products were filtered with 20-nm nylon filters (Osmonic Inc. Magna Nylon, Hydrophilic), washed with 50 mL of different solvents, in the following order: xylene, methanol, ethanol, and ethyl acetate. The resulting gel was first dried at 0.1 Torr and room temperature for 1 h and then at 80 °C for 17 h (Ruiz et al. 2007; Escalada et al. 2014).

Synthesis of the GACON-NP. This synthesis was carried out according to the method reported by Deligiannakis et al. (2012) with some modifications. Two grams of SiO_2 nanoparticles previously derivatized with APTES was suspended with 0.35 g of GA in 100-mL toluene. DDC and N-hydroxysuccinimide were further added as coupler reagents to favor the formation of the peptide bond, in a ratio 1:0.5:1 of DDC, N-hydroxysuccinimide, and GA, respectively (Sehgal and Vijay 1994). The reaction mixture was refluxed in a silicone bath for 22 h and then the products were filtered with 20-nm nylon filters and washed with 50-mL toluene twice, methanol and acetone. An orange gel was obtained which was dried at 0.1 Torr and room temperature for 1 h and then in an oven at 80 °C for 19 h.

Characterization studies The UV-visible spectroscopy analysis was performed by using a diode array spectrophotometer Agilent 8453. Solutions of free GA, GAO-NP, and GACON-NP were prepared in phosphate buffer at pH 7, with GA final concentrations of 3.0×10^{-4}, 1.0×10^{-4}, and 7×10^{-5} mol L^{-1}, respectively. These concentrations are correspondingly equivalent to 0.051 g L^{-1} for free GA, 0.157 g L^{-1} for GAO-NP, and 0.311 g L^{-1} for GACON-NP. Under these conditions, suspensions of the nanoparticles were obtained and corrections for light dispersion were needed. Thus, the extinction spectra were modeled as the sum of the absorption component and a scattering component (as a function of λ^{-n}). The scattering contribution, acquired from a least squares minimization in the region of 400 to

700 nm, was extrapolated to lower wavelengths. The absorption contribution was calculated after subtraction of the scattering component to the absorbance measurement (Ruiz et al. 2007).

In order to characterize the functional groups present in the nanoparticles, Fourier transform infrared spectroscopy (FTIR) was performed on a Thermo Scientific Nicolet 380 FT-IR spectrometer with an ATR sampling accessory Pike MIRacle. Spectra between 550 and 4000 cm^{-1} were recorded for the solid samples with 1 cm^{-1} resolution.

Thermogravimetric (TGA) and differential thermal analyses (DTA) were carried out with Shimadzu thermal analyzers TGA-50 and DTA-50 under synthetic air atmosphere with a flow of 30 mL min^{-1} and heating rate of 5 °C min^{-1}. From the thermogravimetric determinations, the mass drop assigned to the organic groups present in the sample is expressed as the organic group percentage (OG%).

Nuclear magnetic resonance spectra were obtained with a Bruker Avance II 400 spectrometer at room temperature, by assaying approximately 1 g of the solid sample compacted into a 7-mm zirconium oxide rotor. The measurements were performed at 75.47 and 59.61 MHz for carbon and silicon nuclei, with a magic-angle spinning technique at 10 kHz. To increase the signal-to-noise ratio, the cross-polarization technique was applied. NMR spectra of ^{13}C and ^{29}Si were obtained with a pulse repetition of 1 and 3 s and contact times of 1 and 3 ms, respectively. Similar conditions were employed for obtaining NMR spectra of silica nanoparticles modified with other organic groups (Arce et al. 2015). The spectral simulations were performed with ChemDraw Ultra 12.0, Cambridge Software.

Electron paramagnetic resonance (EPR) spectra were obtained in a Bruker ELEXSYS E500T spectrometer operating in the X band with the following measurement conditions: central field, 3484 G; scan width, 10 G; modulation amplitude 0.20 G; sweep time, 10 s; microwave attenuation of 22 dB; microwave frequency, 9.78 GHz; and microwave power, 1287 MW. GA, GAO-NP, and GACON-NP samples with a final concentration of 4×10^{-3} GA mol L^{-1} were analyzed at different pHs regulated with phosphate buffer $HPO_4^{-2}/H_2PO_4^{-1}$ and 0.1 mol L^{-1} NaOH solutions. The simulated spectra were obtained with WINSIM 2002 software.

Stability studies The stability of the GA-functionalized nanoparticles was compared to that of free GA by following their respective UV-visible absorption spectra as a function of time. The spectra were taken in $HPO_4^{-2}/H_2PO_4^{-1}$ buffer of pH 7 at short time intervals (0, 1, 2, 3, and 4 h) and at longer time periods (0, 2, 5, and 10 days).

Antimicrobial activity The antimicrobial activities of GA and GA-functionalized nanoparticles were examined against *P. larvae*. The bacterial strain was isolated from brood combs of beehive (located in the city of Mar del Plata, Buenos Aires, Argentina) with AFB clinical symptoms. Isolations were achieved on Mueller-Hinton broth, yeast extract, glucose, and sodium pyruvate (MYPGP) (Dingman and Stahly 1983) agar supplemented with 9 μg mL^{-1} of nalidixic acid to inhibit *P. alvei* growth and were incubated under microaerobic conditions (5–10% of CO_2). The genotypic identification of the strain was achieved by using PL2-Fw and PL2-Rv primers (Martınez et al., 2010). The pure strain was maintained on MYPGP agar with 15% *v/v* glycerol until used.

The minimal inhibitory concentrations (MICs) of GA and GA-functionalized nanoparticles were determined by the agar dilution method described by Alippi et al. (2007) with some modifications. GA and GA-functionalized nanoparticles were incorporated in melting MYPGP agar yielding dilutions from 10,000 to 78 μg mL^{-1} for GA, from 712 to 5.9 μg mL^{-1} GA for GAO-NP, and from 368 to 24.5 μg mL^{-1} GA for GACON-NP. The final concentration of GA in the functionalized nanoparticle solutions was calculated from the corresponding OG% obtained by TGA. The bacterial suspensions were prepared in saline solution from *P. larvae* grown on MYPGP agar for 48 h at 37 °C, adjusted with Mc Farland scale, and diluted to achieve an inoculum of 10^5–10^6 CFU mL^{-1}. Plates were inoculated with the bacterial suspensions and incubated at 37 °C for 48 h. The MICs were determined as the lowest concentrations inhibiting the visible growth of *P. larvae* on the agar plate. Controls without GA-functionalized nanoparticles with silica nanoparticles free of GA and with OTC control were made. An average pH of ca. 7 was verified in all of them.

In order to evaluate synergic or additive effects between free GA and silica nanoparticles against *P. larvae*, different concentrations of GA were mixed with various amounts of bare nanoparticles in the same agar culture plate before inoculation. To compare the effect of GAO-

NP to that of its separated components, GA in final concentrations between 712 and 5.9 μg mL^{-1} was added to different suspensions of silica nanoparticles (final concentrations from 3288 to 27.2 μg mL^{-1}) so as to keep the proportion according to the OG% of this functionalized nanoparticle. Analogously, GA solutions (final concentrations from 368 to 24.5 μg mL^{-1}) were mixed with bare nanoparticle solutions (final concentrations from 3632 to 241 μg mL^{-1}) correlating the amount of GA and silica found in GACON-NP as given by its OG%. In addition, a mixture of 1250 μg mL^{-1} of GA and 4000 μg mL^{-1} of bare silica nanoparticles was also tested.

Non-parametric tests were used for the statistical analysis of the results by means of Bioestat 5.0 software (Belém, PA., Brazil). The Kruskal-Wallis test complemented by the post hoc test of Dunn was applied to evaluate the statistical differences regarding the antimicrobial activity of the substances. The significance level was set at 5%, $p < 0.05$, for all the tests (Kowalski et al., 2005).

Results and discussion

Characterization of GA-functionalized nanoparticles

The extinction spectra of GA-functionalized nanoparticles in phosphate buffer were recorded in the UV-vis range. The absorption spectra show a band centered around 260 nm, characteristic of free GA at neutral pH (Fig. 1) (Fink and Stong 1982). The occurrence of this band supports the presence of organic chromophores attached to the nanoparticles since SiO_2 does not absorb within this wavelength range. The similarity between the absorption peaks of GA-functionalized nanoparticles in comparison to GA is consistent with the association of the phenolic compound to the silica.

FTIR absorption spectra of free GA, silica NPs (free of GA), and GA-functionalized nanoparticles are compared in Fig. 2. The spectra of both synthetized nanoparticles show peaks in the 1300–1700 cm^{-1} region, which are not observed for bare silica nanoparticles. These additional peaks are also present in the spectra of solid GA. The intensity ratio of the bands due to Si–OH absorption at 3400–3450 cm^{-1} and those assigned to Si–O–Si absorption at 1100 cm^{-1} is smaller for the modified silica particles than for the bare ones.

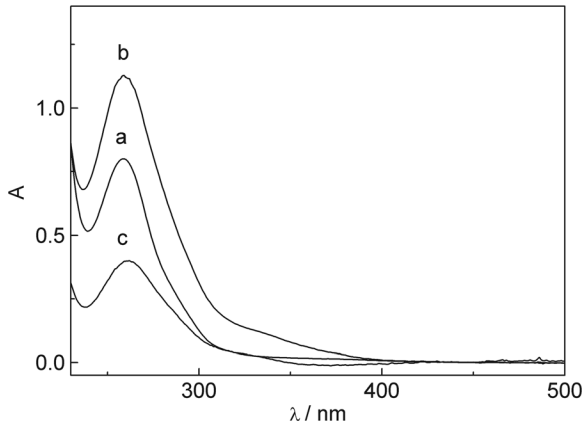

Fig. 1 UV-visible absorption spectrum of **a** free GA (0.051 g L^{-1}), **b** GAO-NP (0.157 g L^{-1}), and **c** GACON-NP (0.311 g L^{-1}) in phosphate buffer (pH 7). Correction parameters for the scattering contribution are given by the equation $y = a + c/\lambda^n$, where a, c, and n are respectively 9.7927×10^{-11}, 653.9000, and 1.4407 for of GAO-NP and -2.4669×10^{-11}, 16.7838, and 0.5673 for GACON-NP

Therefore, a considerable diminution of the amount of silanol groups occurs after functionalization, as

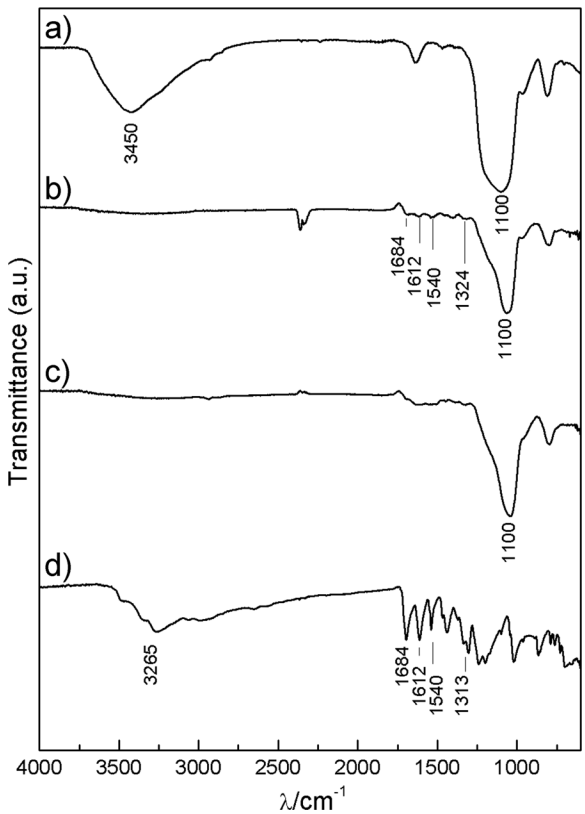

Fig. 2 FTIR spectrum for **a** bare SiO_2 nanoparticles, **b** GAO-NP, **c** GACON-NP, and **d** GA

expected from the covalent bonding between the nanoparticles and the organic molecules. Any absorption due to the vibration modes assigned to Si–O–C bonds is masked by the strong Si–O–Si absorption signals at 1100 cm^{-1} (Arce et al. 2015; Arce et al. 2012).

The lower intensity of the absorption bands for the functionalized silica due to GA moiety is explained by the lower concentration of the organic acid present in the hybrid systems. The 1324, 1400, 1535, and 1612 cm^{-1} peaks in the spectrum of GAO-NP are assigned to C=C stretching and CH in plane deformation vibrations of the aromatic ring of GA (Zieglera and Billes 2002). The peak at 1684 cm^{-1} is assigned to the stretching C=O from the COOH functional group in the GA moiety. However, the absorption peak at the C–O frequency is not evident, probably because of the low intensity of the band and the overlap with the broad band due to the Si–O modes. The FTIR spectrum for GACON-NP shares a similar pattern with that of GAO-NP, although the peaks at the 1500 and 1640 cm^{-1} region are hardly resolved probably due to the poorer amount of GA bonded to these nanoparticles.

It is important to note that the peak at 1684 cm^{-1} in the spectrum of GA due to the C=O stretching of the COOH bond is not observed in the case of GACON-NP, as expected. Instead, the absorptions of the new bond generated in the synthesis, the C=O and C–N stretching from the amide functional group, may appear at lower wave numbers (1670–1630 cm^{-1}) (Deligiannakis et al. 2012). However, these peaks are not well resolved because of the low intensity of the broad band due to Si–O in the nanoparticle spectrum.

Besides, the spectrum of GA shows a broad band around 3400 cm^{-1} arising from the phenolic OH stretching. In this frequency range, the OH vibrational mode of silanols is also active, although only a slight absorption band was observed in the spectra of both nanoparticles. It should be considered that changes in the vibration frequencies could be associated with the generation of hydrogen bridge bonds between the OH in GA and unreacted silanol groups or with any further reaction that may occur after the covalent binding of the acid to the silica (Tóth et al. 2014).

The thermogravimetric curves for both functionalized nanoparticles (Fig. 3) account for a mass loss on increasing the temperature to about 100 °C. This change corresponds to the removal of residual solvents used in the synthesis that may have remained on the nanoparticles. These organic molecules, together with water from room humidity, can easily interact with the silanol groups available on the silica surface through the formation of hydrogen bonds. Mass loss at temperatures above 200 °C is attributed to degradation of the organic groups linked to the nanoparticle surface. A sharp drop of the mass is observed for GAO-NP (Fig. 3a) up to stabilize at about 600 °C. This decrease may be attributed to the amount of GA covalently bonded to the silica.

The thermogram for GACON-NP (Fig. 3b) looks similar to the one described above. However, in this case, four decomposition steps are distinguished in the thermogravimetric curve. The first step, from room temperature to 100 °C, corresponds to the elimination of solvents as mentioned above. The second and third steps comprise the mass losses between 170 and 290 °C and from there to 700 °C, which are related to the organic molecules attached to the silica. These two mass drops arise from the decompositions of APTES (previously estimated in 9.8 OG% by Arce et al. (2012)) and GA. The last stage, from 700 to 800 °C, is attributed to the condensation of silanols that generate siloxane bonds as a result of the thermal decomposition of the silica.

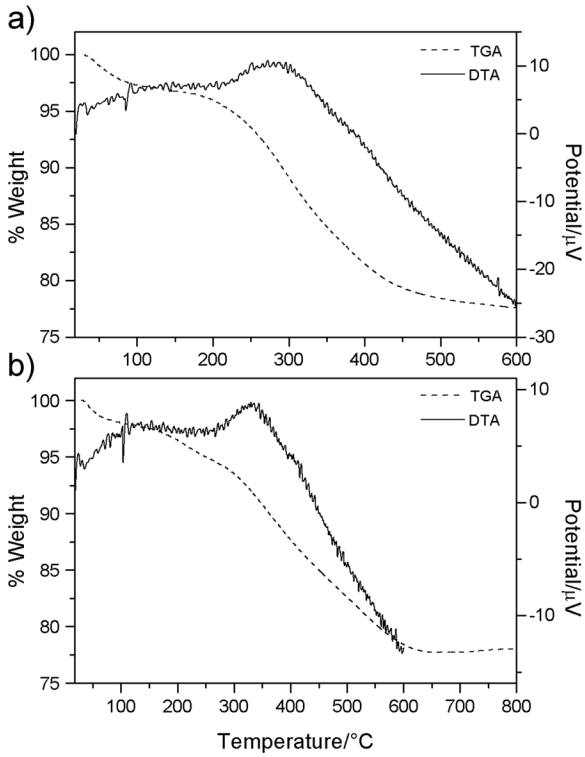

Fig. 3 TG curves (*dotted line*) and DTA thermograms (*solid line*) for **a** GAO-NP and **b** GACON-NP

The percentages of organic groups (%OG, *w*/*w*) for the functionalized nanoparticles were calculated from the thermogravimetric curves yielding 17.8% for GAO-NP and 9.2% for GACON-NP. Comparable values have been reported for silica nanoparticles derivatized with GA (6–25%) (Deligiannakis et al. 2012; Hu et al. 2013) and for SiO_2 nanoparticles attached to alcohols (8–10%) (Ruiz et al. 2007; Arce et al. 2012).

The curves obtained by DTA show an exothermic peak when samples are burned around 300 °C (GAO-NP) and 350 °C (GACON-NP), corroborating the decomposition of GA in the presence of air. Weight losses from the desorption of the solvent should correlate with endothermic peaks; however, it is likely that the temperature changes associated with this process are minor and below the detection limit of the instrument.

In order to assess the success of the functionalization of the silica nanoparticles, ^{13}C and ^{29}Si NMR experiments in solid samples of GA derivatized nanoparticles and free GA were performed, respectively (Figs. 4 and 5). For the GA sample, all the ^{13}C NMR signals expected from the structure are observed (Fig. 4a). According to the numbered chemical structure in Fig. 4a, the signals are attributed as follows: 143.3 ppm (C3 and C5 of the aromatic ring), 110.3 ppm (C2 and C6), 121.5 ppm (C1), and 135.5 ppm (C4). These values are coincident with those described by Wawer and Zielinska (1997). The simulated spectra (Figure ESM 1 in the Electronic Supplementary Material) yielded values with slight displacements between 3 and 5 ppm approximately (C3 and C5 146.1 ppm, C2 and C6 113.3 ppm, C1 125.6 ppm, and C4 141.2 ppm) but have better accuracy for the carboxylic carbon (C7: 169.3 ppm). In addition, the experimental spectrum shows two minor peaks at 118.1 ppm and 174.9 that may arise from impurities of the original sample and some proportion of ionized GA derivatives. In fact, trigallic acid is a common impurity in commercial GA which, according to previous reports, could account for a peak around 117 ppm (Wang et al. 2007). The other peak could be attributed to the presence of anionic species (gallate or trigallate) that, according to our simulations of the ^{13}C NMR spectra, yield higher shifts (ca. 177 ppm) for the carboxylate group.

The ^{13}C NMR spectrum for GAO-NP shows nine bands (Fig. 4b). Two of them (174.9 and 118.1 ppm) correspond to those ascribed to the impurities of the GA sample. In order to assign the remaining signals, two NMR spectrum simulations were carried out for structures in which the GA is attached to silica in *para* or in *meta* position, alternatively (Figures ESM 2 and ESM 3). The simulated NMR spectrum for GA bonded to silica in para position (Figure ESM 2) shows few differences with respect to the simulation for free GA, being significant the shifts of the absorptions due to C3 and C5 (146.1 to 148.6 ppm) and to C4 (141.2 to 136.9 ppm). The simulation for the structure linking silica to GA in meta position (Figure ESM 3) yields lines comparable to those obtained from the simulation for free GA (Figure ESM 1). The main difference is found in the signals due to C2 and C6 at 113.3 and 110 ppm, which are not equivalent according to the location of the bonding to silica. The experimental

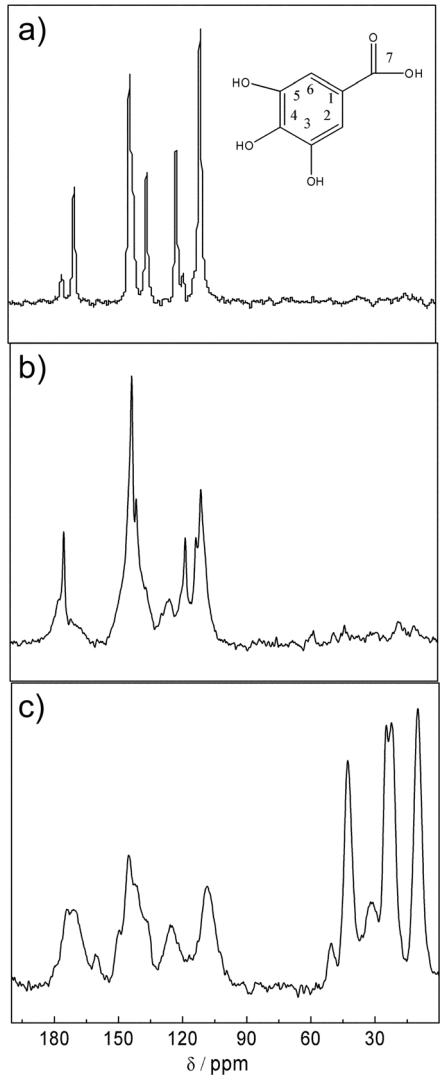

Fig. 4 ^{13}C NMR spectrum for **a** GA, **b** GAO-NP, and **c** GACON-NP

spectrum shows similar values (C1 125.6 ppm; C3–C5 143.17 ppm; C7 171.6 ppm) and exhibits the unfolded signals at 113.3 and 110 ppm of C2–C6 according to the meta bonding. In addition, the signal attributed to C4 did not show the displacement toward lower densities as predicted for the para-substituted structure. Instead, the experimental value of C4 better matches the estimation for the meta-structure (141.2 ppm).

In summary, this analysis confirms the functionalization of SiO_2 by a covalent bond in the meta position of GA, although a minor proportion of the structure with GA linked in the para position cannot be discarded.

The ^{13}C NMR results for GACON-NP (Fig. 4c) include signals at 50, 43, 25, 22, and 10 ppm that correspond to the APTES fragment, in agreement with the simulated lines for the structure shown in Figure ESM 4: 58, 44, 25, 18, and 16 ppm. The signals assigned to C1 (126.1 ppm) and C2–C6 (108.9 ppm) are both comparable to the experimental results. Similarly, the predicted value for C7 (167.5 ppm) is close to the experimental signal at 171 ppm. The C3–C5 signals at 146.3 ppm could be overlapping the line due to C4 (139.4 ppm) in the experimental spectrum. The signal at 174 ppm is coincident with that observed for free GA and ascribed to an impurity.

The ^{29}Si solid state NMR spectroscopy provides evidence about the features of silicon atoms in the nanoparticles. The ^{29}Si NMR spectrum for GAO-NP (Fig. 5, inset) shows a unique peak at −109.36 ppm. This chemical shift is in agreement with previous reports about silicon atoms in siloxane networks denoted as $Si(OSi\equiv)_4$. The peak shoulder to lower shift values can be assigned to unreacted silanol groups on the nanoparticle surface which absorb at −99 and −100 ppm (Silva et al. 1999; Sales et al. 2007). These results support the chemical structure assigned to GAO-NP.

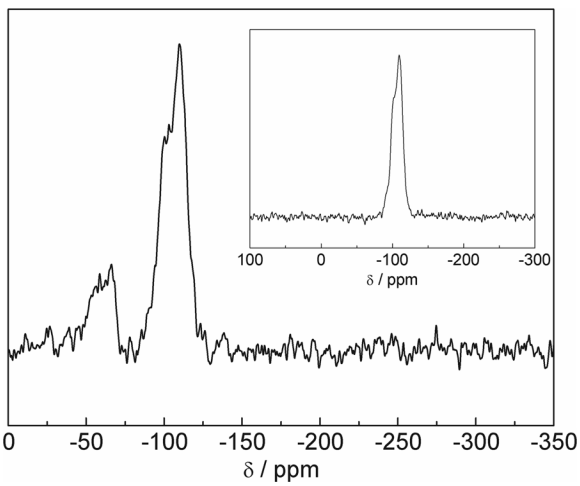

Fig. 5 ^{29}Si NMR spectrum for GACON-NP. Inset: ^{29}Si NMR spectrum for GAO-NP

On the other hand, the ^{29}Si NMR spectrum for GACON-NP in Fig. 5 shows an additional peak with lower intensity at −66.10 ppm, apart from that at −109.67 due to siloxane groups. Chemical shifts at −64 and −66 ppm have been reported for $R\text{-}Si(OSi\equiv)_3$ groups, where R stands for a short saturated carbon chain (Silva et al. 1999; Sales et al. 2007). Thus, this small peak can be attributed to Si bonded to the aminopropyl fragment in the APTES moiety of the nanoparticle, in consistence with the structure assigned to GACON-NP in Figure ESM 4.

Free radical production from GA-functionalized nanoparticles

The free radical production from GA-functionalized nanoparticles was compared to that from free GA by EPR for 4×10^{-3} GA mol L^{-1} solutions at different pHs. At pH 3 and 7, no EPR signal attributable to free radicals was observed, whereas different spectra can be recognized at pH 11 (Figs. 6 and 7). This is consistent with the reports from Eslami et al. (2010) indicating that acidic pH conditions inhibit the generation of stable radicals from GA with non-ionized phenolic OH. However, at pH 9, GA radical is stabilized and lives long enough to be detected.

The EPR spectrum for free GA at pH 11 buffer solution (Fig. 6a) evidences that a mixture of species is probably present under this condition. The simulated spectrum (Fig. 6b) considers main contributions from two different GA-derived radical structures: the monoanion and the dianion of the gallate group, which correspond to the deprotonation of the phenolic OH. Such structures have also been associated with the EPR signals from various catechin gallates in alkaline medium (Hagerman et al. 2003; Severino et al. 2009).

According to the reports from Eslami and from Yoshioka, under rather strong alkaline pH (lower than 13), some of the OH groups of GA may keep protonated and a slow exchange of the H^+ between phenolic oxygens is feasible (Eslami et al. 2010; Yoshioka et al. 2003). This mechanism explains the different hyperfine

splitting arising from the ring protons, as those assigned to the GA monoanion in the simulated spectrum.

The intensity of the EPR spectrum obtained for GAO-NP in alkaline solution (Fig. 7a) is similar to that for free GA (Fig. 6). However, its hyperfine structure is quite diverse. The signal can be approximately reproduced by simulation in terms of radical species from the two isomers, para and meta. In consistence with the results from ^{13}C NMR, the major contribution in the simulated spectrum is given by GA attached to the silica by the OH group in meta position where approximately 37% of the structures are protonated and another 33% corresponds to gallate dianion. The other ca. 30% can be explained by the structures with para-substituted GA moiety with and without protonated phenolic OH. The apparent hyperfine splitting constants used in the simulation are detailed in the caption of Fig. 7c.

The EPR spectrum for GACON-NP (Fig. 7d) is compatible with non-equivalent hyperfine splitting constants from the H atoms in the ring. This situation arises when considering a dominant contribution from a semiquinone radical with a slowly exchanging proton, analogous to that proposed for the free GA radical, and a minor proportion of a radical where all the phenolic hydroxyl groups are ionized, as shown in the chemical sketches from Fig. 7f.

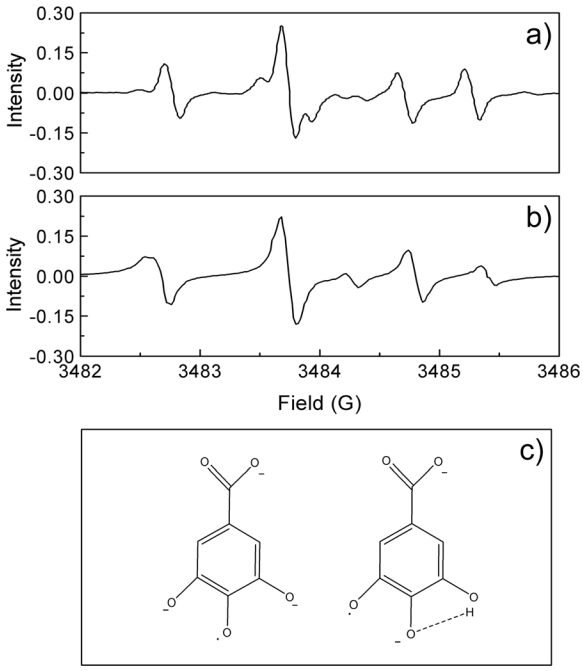

Fig. 6 **a** EPR spectrum of free GA in buffer solution at pH 11; **b** simulated spectrum considering a mixture of two radicals: the gallate dianion (19%) with hyperfine splitting constants of $a_{H2} = a_{H6} = 1.363$ G and GA monoanion (81%) with apparent hyperfine splitting constants of $a_{H2} = 0.666$ G, $a_{H6} = 0.168$ G, and $a_{OH} = 0.04$ G

In summary, EPR spectra corroborate that GA associated to silica generates free radicals in the presence of air in alkaline pH but not under acidic or neutral conditions. Finally, the analysis of the spectral information for the radical species detected at pH 10 supports the structural features of the synthetized nanoparticles.

Stability studies of GA-functionalized nanoparticles

The stability of GA associated with the nanoparticles was examined as well. Spectral changes in aqueous solutions of GA and in suspensions of each of the functionalized nanoparticles were followed along increasing storage times (Figure ESM 5). The absorbance at 260 nm decayed progressively for all the samples along the 10-day lapse. For free GA, the absorbance decreased around 33% in 2 days; for GAO-NP and GACON-NP, the drop after 5 days was 20 and 10%, respectively. In addition, new absorption bands of low intensity appeared at higher wavelengths, which have been assigned to GA oxidation products and GA dimers. However, no significant differences in the absorption features of free GA and GA-functionalized NP solutions in phosphate buffer at pH 7 were observed at shorter times (data not shown).

These results demonstrate that GA is relatively stabilized when linked to silica nanoparticles since both kinds of association, represented by GAO-NP and GACON-NP, significantly retard the oxidation of the phenolic compound under ambient conditions.

Antimicrobial activity of GA-functionalized nanoparticles

GA-functionalized nanoparticles inhibited the growth of the *P. larvae* strain with MIC values of 178 μg GA mL^{-1} for GAO-NP and 92 μg GA mL^{-1} for GACON-NP (Table 1). Identical treatment with silica nanoparticles without GA derivatization yielded counts of *P. larvae* similar to positive controls, this confirming that SiO_2 can be considered harmless to the bacteria. In addition, when free GA was mixed in the same agar culture plate with bare silica nanoparticles in the concentration ratios and ranges studied for GAO-NP and for GACON-NP, no antimicrobial activity was observed. The same result was obtained for the mixture of 1250 μg mL^{-1} of GA

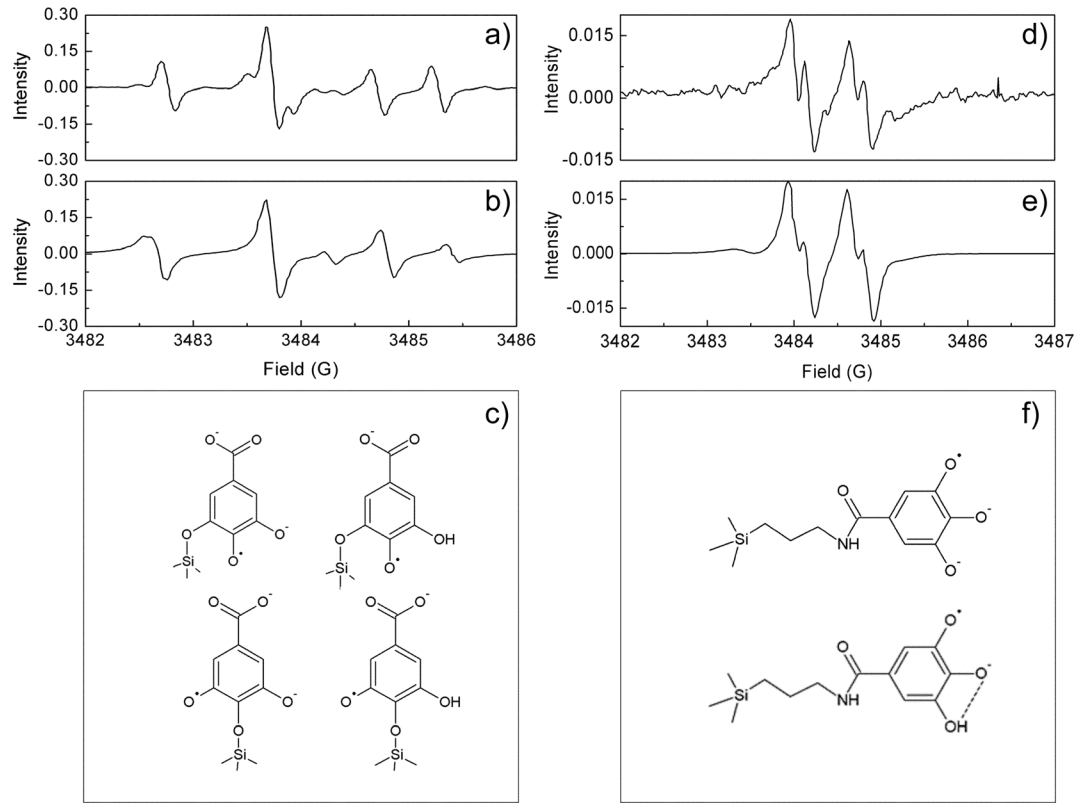

Fig. 7 **a** EPR spectrum of GAO-NP in buffer solution at pH 11; **b** simulated spectrum considering a mixture of the radicals shown in **c**: the *meta*-substituted gallate dianion (33.33%, hyperfine splitting constants: a_{H2} = 1.06 G; a_{H6} = 1.05 G); the meta-substituted gallate monoanion (37.18%, hyperfine splitting constants: a_{H2} = 1.01 G; a_{H6} = 1.08 G; a_{OH} = 0.07 G); the *para*-substituted gallate dianion (7.30%, hyperfine splitting constants: a_{H2} = 1.12 G; a_{H6} = 1.68 G); and the para-substituted gallate monoanion (22.22%, hyperfine splitting constants: a_{H2} = 1.33 G; a_{H6} = 1.60 G; a_{OH} = 0.06 G); **d** EPR spectrum of GACON-NP in buffer solution at pH 11; **e** simulated spectrum considering contributions from the species shown in **f**: a totally ionized semiquinone radical (16.61%, hyperfine splitting constants: a_{H2} = 0.88 G; a_{H6} = 0.80 G) and a monoanionic semiquinone radical with an exchanging proton (83.39%, hyperfine splitting constants: a_{H2} = 0.677 G; a_{H6} = 0.166 G; a_{OH} = 0.02 G)

(the largest concentration without growth inhibition observed for free GA) and 4000 μg mL^{-1} of non-functionalized silica nanoparticles (around its solubility value).

Table 1 Minimum inhibitory concentrations (MICs) for GA, GAO-NP, and GACON-NP against *P. larvae*

Antimicrobial agent	MIC[a] μg mL^{-1} GA[b]
GA	2500
GAO-NP	178
GACON-NP	92

[a] Averaged values from triplicate determinations of the antimicrobial activity

[b] The final concentration of GA in the functionalized nanoparticles was calculated by considering the OG%

This strain showed sensibility to free GA with MIC of 2500 μg mL^{-1}, thus comprised in the range of 300–2500 μg mL^{-1} reported for other Gram-positive bacteria (Borges et al. 2013; Taguri et al. 2006). However, the antimicrobial activity of free GA is low, considering the limits of MIC generally accepted for antimicrobial phytochemical compounds (100 to 1000 μg mL^{-1}). Moreover, the antimicrobial activity of free GA against *P. larvae* is poor in comparison to that of phenolic essential oils such as thyme and oregano which exhibit MIC values within 250 to 450 μg mL^{-1} against the same pathogen (Alippi et al. 1996).

The antimicrobial levels of silica-bonded GA are between 14 and 27 times higher and fall within the range of other antimicrobial phytochemicals. In fact, the growth of this *P. larvae* strain was inhibited by GA-functionalized nanoparticles in concentrations

comparable to those found for the essential oil of cinnamon, considered as a natural antimicrobial with very good activity against this microorganism (Gende et al. 2008).

Seil and Webster (2012) recognized that nanostructures may have multiple mechanisms of antibacterial activity that still lack full understanding. The way of the interaction may rely on the release of inherently antibacterial materials from the surfaces, and therefore, the efficiency usually relates to particle size and shape. Also, the physical properties of the nanoparticle may enhance cell wall penetration or membrane damage; alternatively, the chemical ability to produce bactericidal ROS can be involved.

According to the study by Jiang et al. (2009), SiO_2 and other oxide nanoparticles show a greater tendency to attach to the cell walls than do the respective microscaled oxides, this contributing to the higher toxicity of the nanostructures to different bacteria.

Borges et al. (2013) observed that GA and ferulic acid affect the integrity of Gram-positive and Gram-negative bacteria cell membranes by generating changes in their permeability barriers. They suggest that the hydrophobicity of the cytoplasmic membrane is altered. Phenolic acids probably attach to the membrane by their hydrophobic nature and then enter the cell by passive diffusion, partially acidifying the membrane and the cytoplasm. This localized acidification modifies the phospholipid charges and produce protein denaturation, generating ruptures in the cell membrane. Thus, acidification changes the membrane leading to irreversible alterations of the permeability and causing cell death. A negative correlation with the ionization capability of the molecule has also been found for a series of phenolic acids, this also suggesting that the higher solubility of the neutral species in the membrane enhances the antibacterial effect (Ramos-Nino et al. 1996).

It has also been reported that epigallocatechin gallate disrupts the liposome membrane and produces losses inside it, and membrane fractions aggregate. The formation of multicellular aggregates was observed with epicatechin gallate against *Staphylococcus aureus* (Cushnie and Lamb 2005).

Alvarez et al. (2010) reported that GA bound to gold nanoparticles enhances their bactericidal activity. They propose that the nanoparticles facilitate the transport of the phenolic acid into the cell where the damages in the membrane are induced more efficiently.

As regards our derivatized nanoparticles, the increase in the antimicrobial activity may be due to the improvement of the transport into the cell that probably disposes larger local concentrations of GA, thus enhancing membrane disruption mechanisms. The results of challenging *P. larvae* by adding both free GA and bare nanoparticles to the same culture plate indicate that the increment of the antimicrobial activity cannot be explained by synergic or additive effects between the phenolic compound and the nanostructured silica, then supporting our view.

The sites and number of hydroxyl groups on phenolic compounds have been correlated with their relative toxicity to microorganisms, pointing to an increasing activity upon larger hydroxylation (Cowan 1999). This would suggest that GACON-NP (with three free OH groups) may show increased antimicrobial activity in comparison to GAO-NP (with two free OH groups). However, the statistical analysis afforded no significant differences between MIC values for GAO-NP and GACON-NP at $p < 0.05$. The comparable level of antimicrobial activity for both materials leads to conclude that the different functional groups involved in the association of GA to SiO_2 do not modify enough the effects related to the bacterial death. On the other hand, the antimicrobial activity observed for GA and GA nanoparticles at pH ca. 7 can hardly be attributed to reactive products of GA oxidation (ROS or GA-derived radicals), which were only observed under alkaline conditions.

Conclusions

Different silica nanoparticles functionalized with GA were synthesized by condensation of hydroxyl or carboxyl groups of GA, yielding in each case GAO-NP and GACON-NP with 18 and 9% of organic mass, respectively. The attachment of GA to this inert support increases the stability of the polyphenol against oxidation, though retaining the capacity to produce free radicals in alkaline conditions.

Besides, GA bonding to the silica strengthens the antibacterial activity against *P. larvae* with MIC values in the range of antimicrobial phytochemical agents (Cushnie and Lamb 2005). In comparison to free GA, the antimicrobial activity for GAO-NP and GACON-NP is 14 and 27 times higher, respectively. This behavior could be explained in terms of more efficient interactions of the nanostructures with the bacteria cell wall.

Further work is underway to assess the activity of these functionalized nanoparticles in vivo on honeybees and their use in the field as an alternative treatment for AFB. Finally, independently of the type of linking to the SiO_2 nanoparticle, GA shows improved properties for the application tested.

Acknowledgement M.S.C. thanks the financial support from CONICET (PIP-0211) and UNMDP (15-E710). This work was partially supported by ANPCyT (PICT 2012–1817). V.B.A. and D.O.M. are research members from CICPBA. The authors thank Rodrigo Parra and Martín Lere for the thermogravimetric and thermal analyses.

References

Alippi AM, López AC, Reynaldi FJ, Grasso DH, Aguilar OM (2007) Evidence for plasmid-mediated tetracycline resistance in *Paenibacillus larvae*, the causal agent of a honey bee larval disease. Vet Microbiol 125:290–303

Alippi AM, Ringuelet JA, Cerimele EL, Re MS, Henning CP (1996) Antimicrobial activity of some essential oils against *Paenibacillus larvae*, the causal agent of American foulbrood disease. J Herbs Spices Med Plants 4:9–16

Antúnez K, Harriet J, Gende L, Maggi M, Eguaras M, Zunino (2008) Efficacy of natural propolis extract in the control of American foulbrood. Vet Microbiol 131:324–331

Arce VB, Bertolotti SG, Oliveira FJ, Airoldi C, Arques A, Santos JL, Gonzalez MC, Cobos CJ, Allegretti PE, Mártire DO (2012) Triplet state of 4-methoxybenzyl alcohol chemisorbed on silica nanoparticles. Photochem Photobiol Sci 11:1032–1040

Arce VB, Gargarello RM, Ortega F, Romañano V, Mizrahi M, Ramallo-López JM, Cobos CJ, Airoldi C, Bernardelli C, Donati ER, Mártire DO (2015) EXAFS and DFT study of the cadmium and lead adsorption on modified silica nanoparticles. Spectrochim Acta Part A Mol Biomol Spectrosc 151:156–163

Borges A, Ferreira C, Saavedra MJ, Simoes M (2013) Antibacterial activity and mode of action of ferulic and gallic acids against pathogenic bacteria. Drug Resistance 19:256–265

Borges A, Saavedra MJ, Simoes M (2015) Insights on antimicrobial resistance, biofilms and the use of phytochemicals as new antimicrobial agents. Curr Med Chem 22:2590–2614

Cho YS, Kim SK, Ahn CB, Je JY (2011) Preparation, characterization, and antioxidant properties of gallic acid-grafted-chitosans. Carbohydr Polym 83:1617–1622

Cirillo G, Kraemer K, Fuessel S, Puoci F, Curcio M, Spizzirri UG, Altimari I, Iemma F (2010) Biological activity of a gallic acid-gelatin conjugate. Biomacromolec 11:3309–3315

Cowan MM (1999) Plant products as antimicrobial agents. Clinic Microbiol Rev 12:564–582

Cushnie TP, Lamb AJ (2005) Antimicrobial activity of flavonoids. Int J Antimicrob Agents 26:343–356

Deligiannakis Y, Sotiriou GA, Pratsinis SE (2012) Antioxidant and antiradical SiO_2 nanoparticles covalently functionalized with gallic acid. Appl Mater Interfaces 4:6609–6617

Dingman DW, Stahly DP (1983) Medium promoting sporulation of *Bacillus larvae* and metabolism of medium components. Appl Environ Microb 46:860–869

Escalada JP, Arce VB, Porcal GV, Biasutti MA, Criado S, García NA, Mártire DO (2014) The effect of dichlorophen binding to silica nanoparticles on its photosensitized degradation in water. Water Res 50:229–236

Eslami AC, Pasanphan W, Wagner BA, Buettner GR (2010) Free radicals produced by the oxidation of gallic acid: an electron paramagnetic resonance study. Chem Cen J 4:1–4

Fang Z, Bhandaria B (2010) Encapsulation of polyphenols. A review Trends Food Sci Tech 21:510–523

Fink DW, Stong JD (1982) The electronic spectral properties of gallic acid. Spectrochim Acta 8:1295–1298

Friedman M, Jurgens HS (2000) Effect of pH on the stability of plant phenolic compounds. J Agric Food Chem 48:2101–2110

Gende LB, Floris I, Fritz R, Eguaras MJ (2008) Antimicrobial activity of cinnamon (*Cinnamomum zeylanicum*) essential oil and its main components against *Paenibacillus larvae* subsp. *larvae*. Bull. Insectol 61:1–4

Genersch E (2010) American foulbrood in honeybees and its causative agent, Paenibacillus larvae. J Invertebr Pathol 103:S10–S19

Hagerman AE, Dean RT, Davies MJ (2003) Radical chemistry of epigallocatechin gallate and its relevance to protein damage. Arch Biochem Biophys 414:115–120

Hu H, Nie L, Feng S, Suo J (2013) Preparation, characterization and in vitro release study of gallic acid loaded silica nanoparticles for controlled release. Pharmazie 68:401–405

Jiang W, Mashayekhi H, Xing B (2009) Bacterial toxicity comparison between nano- and micro-scaled oxide particles. Environ Pollution 157:1619–1625

Kowalski RP, Yates KA, Romanowski EG, Karenchak LM, Mah FS, Gordon J (2005) Ophthalmologist's guide to understanding antibiotic susceptibility and minimum inhibitory concentration. Ophthalmology 112,:1–6.

Marino T, Galano A, Russo N (2014) Radical scavenging ability of gallic acid toward OH and OOH radicals. Reaction mechanism and rate constants from the density functional theory J Phys Chem B 118:10380–10389

Martınez J, Simon V, Gonzalez B, Conget PA (2010) Real-time PCR-based strategy for the detection of *Paenibacillus larvae* vegetative cells and spores to improve the diagnosis and the screening of American foulbrood. Lett Appl Microbiol 50:603–610

Mochizuki M, Yamazaki S, Kano K, Ikeda T (2002) Kinetic analysis and mechanistic aspects of autoxidation of catechins. Biochim Biophys Acta 1569:35–44

Moreno Alvarez SA, Martínez Castañón GA, Niño Martínez N, Reyes Macías JF, Patiño Marín N, Loyola Rodríguez JP, Ruiz F (2010) Preparation and bactericide activity of gallic acid stabilized gold nanoparticles. J Nanopart Res 12:2741–2746

Olga G, Styliani C, Ioannis RG (2015) Coencapsulation of ferulic and gallic acid in HP-β-cyclodextrin. Food Chem 185:33–40

Ramos-Nino ME, Clifford MN, Adams MR (1996) Quantitative structure activity relationship for the effect of benzoic acids,

cinnamic acids and benzaldehydes on *Listeria monocytogenes*. J Appl Bacteriol 80:303–310

Ruiz AE, Caregnato P, Arce VB, Schiavoni M, Mora VC, Gonzalez MC, Allegretti PE, Mártire DO (2007) Synthesis and characterization of butoxylated silica nanoparticles. Reaction with benzophenone triplet states. J Phys Chem C 111:7623–7628

Sales JA, Petrucelli GC, Oliveira FJ, Airoldi CJ (2007) Mesoporous silica originating from a gaseous ammonia epoxide ring opening and the thermodynamic data on some divalent cation adsorptions. J Colloid Interface Sci 315:426–433

Sanchez-Maldonado AF, Schieber A, Ganzle MG (2011) Structure-function relationships of the antibacterial activity of phenolic acids and their metabolism by lactic acid bacteria. J Appl Microbiol 111:1176–1184

Sehgal D, Vijay IK (1994) A method for the high efficiency of water-soluble carbodiimide-mediated amidation. Anal Biochem 218:187–191

Seil JT, Webster TJ (2012) Antimicrobial applications of nanotechnology: methods and literature. Int J Nanomedicine 7: 2767–2781

Severino JF, Goodman BA, Kay CWM, Stolze K, Tunega D, Reichenauer TG, Pirker KF (2009) Free radicals generated during oxidation of green tea polyphenols: electron paramagnetic resonance spectroscopy combined with density functional theory calculations. Free Rad Biol Med 46:1076–1088

Silva CR, Jardim ICSF, Airoldi CJ (1999) New stationary phase prepared by immobilization of a copperamine complex on silica and its use for high performance liquid chromatography. J High Resol Chromatogr 22:103–108

Taguri T, Tanaka T, Kouno I (2006) Antibacterial spectrum of plant polyphenols and extracts depending upon hydroxyphenyl structure. Biol Pharm Bull 29:2226–2235

Tóth IY, Szekeres M, Turcu R, Sáringer S, Illés E, Nesztor D, Tombácz E (2014) Mechanism of in situ surface polymerization of gallic acid in an environmental-inspired preparation of carboxylated core-shell magnetite nanoparticles. Langmuir 30:15451–15461

Wang KJ, Yang CR, Zhang YJ (2007) Phenolic antioxidants from the fresh young leaves of *Toona sinensis*. Food Chem 101: 365–371

Wawer I, Zielinska A (1997) ^{13}C-CP-MAS-NMR studies of flavonoids. I. Solid-state conformation of quercetin, quercetin S-sulphonic acid and some simple polyphenols. Solid State Nucl Magn Reson 10:33–38

Yoshioka H, Ohashi Y, Fukuda H, Senba Y, Yoshioka H (2003) Spectral simulation of the ESR spectra of polyphenol radicals formed by reaction with hydroxyl radical. J Phys Chem A 107:1127–1132

Zieglera I, Billes F (2002) Vibrational spectroscopic calculations on pyrogallol and gallic acid. J Mol Struct (THEOCHEM) 618:259–265